ACS Macro Letters

Letter

pubs.acs.org/macroletters

Truncated Wedge-Shaped Nanostructures Formed from Lateral Microphase Separation of Mixed Homopolymer Brushes Grafted on 67 nm Silica Nanoparticles: Evidence of the Effect of Substrate Curvature

Jonathan M. Horton,[†] Saide Tang,[‡] Chunhui Bao,[†] Ping Tang,[§] Feng Qiu,[§] Lei Zhu,*[,‡] and Bin Zhao*[,†]

[†]Department of Chemistry, University of Tennessee, Knoxville, Tennessee 37996, United States

[‡]Department of Macromolecular Science and Engineering, Case Western Reserve University, Cleveland, Ohio 44106, United States

[§]Department of Macromolecular Science, Fudan University, Shanghai 200433, China

Supporting Information

ABSTRACT: Mixed poly(*tert*-butyl acrylate) (P*t*BA)/polystyrene (PS) brushes with controlled molecular weights and narrow polydispersities were synthesized from asymmetric difunctional initiator (Y-initiator)-functionalized 67 nm silica nanoparticles by sequential surface-initiated atom transfer radical polymerization of *t*BA at 75 °C and nitroxide-mediated radical polymerization of styrene at 120 °C in the presence of a free initiator in each polymerization. The Y-initiator-functionalized nanoparticles were prepared by the immobilization of a triethoxysilane-terminated Y-initiator onto the surface of 67 nm silica particles via an ammonia-catalyzed hydrolysis and condensation process. Transmission electron microscopy studies showed that mixed P*t*BA/PS brushes grafted on 67 nm silica nanoparticles with comparable molecular weights for the two polymers underwent lateral microphase separation after being cast from $CHCl_3$ and annealed with $CHCl_3$ vapor, producing distinct truncated wedge-shaped nanostructures. In contrast, under the same conditions, mixed P*t*BA/PS brushes grafted on 160 nm silica particles self-assembled into nanodomains with a more uniform width. This suggests that the truncated wedge-shaped nanostructures formed by mixed brushes on 67 nm silica nanoparticles originated from a higher substrate curvature.

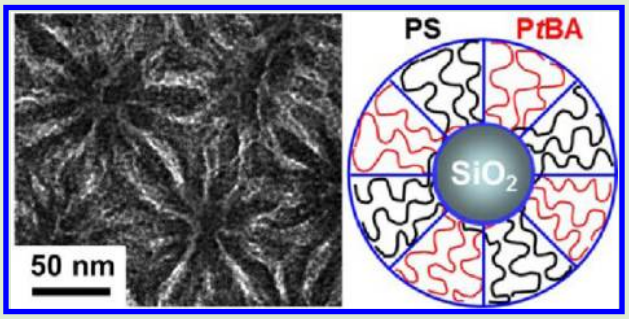

Binary mixed homopolymer brushes are composed of two chemically distinct homopolymers randomly or alternately grafted by one end via a covalent bond on a solid substrate.[1−10] These brushes have shown great potential in a variety of applications due to their ability to exhibit different properties in response to environmental changes. Driven by the minimization of the system's free energy, mixed homopolymer brushes can self-assemble into various intriguing nanostructures under different conditions. These nanostructures are fully reversible because of the covalent grafting of polymer chains on the substrate. The responsive properties of mixed brushes have been intensively studied since Sidorenko et al. reported the first synthesis of mixed polystyrene (PS)/poly(2-vinyl pyridine) brushes grafted on silicon wafers.[8−10]

We have been particularly interested in the fundamental understanding of how two grafted homopolymers microphase separate from each other and how various parameters affect the morphology of mixed brushes.[10,11] Marko and Witten theoretically studied whether symmetric mixed homopolymer brushes undergo lateral microphase separation, forming a "rippled" morphology, or vertical phase separation, producing a "layered" nanostructure under equilibrium melt conditions.[1] They predicted that the "rippled" nanostructure should appear.[1] Further theoretical and computer simulation studies by other researchers have shown that by tuning the chemical compositions, chain lengths, and grafting densities of two tethered polymers as well as the geometry and curvature of substrates many interesting morphologies are possible.[2,4−7] In particular, when the polymer chains are grafted on sub-100 nm nanoparticles, the microphase separation of mixed brushes could be influenced by the substrate curvature. One can imagine that the polymer chains are less crowded and stretched at the exterior of the brush layer than at the interior close to the grafting sites. Using computer simulations, Roan[6] and we[7] studied the self-assembly of mixed brushes on nanospheres with sizes similar to those of polymer chains and found that the morphology evolved from layered to various ordered polyhedral and rippled nanostructures with the change of relative grafting densities or relative chain lengths of two polymers. Due to the spherical geometry and the high curvature, the formation of truncated wedge-shaped nano-

Received: June 22, 2012
Accepted: July 30, 2012
Published: August 3, 2012

Scheme 1. Schematic Illustration of the Synthesis of Mixed P*t*BA/PS Brushes Grafted on 67 nm Silica Nanoparticles (NPs) by Sequential Surface-Initiated Atom Transfer Radical Polymerization (ATRP) and Nitroxide Mediated Radical Polymerization (NMRP)

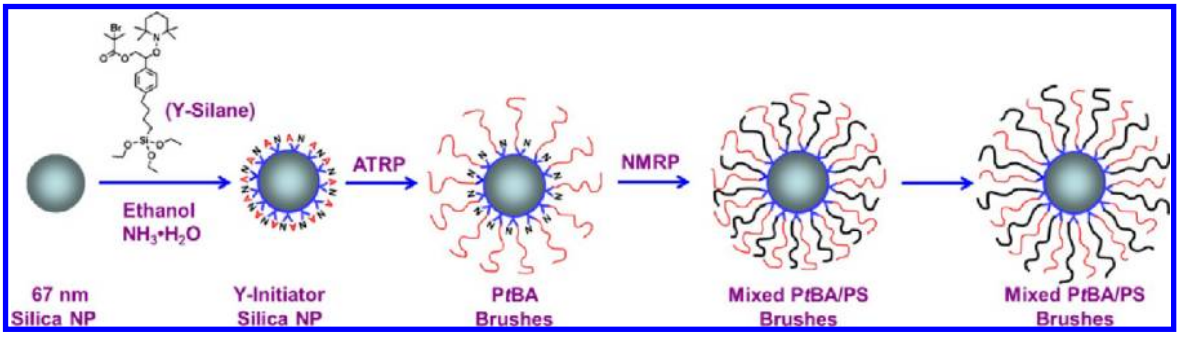

domains instead of nanostructures with a uniform width from the surface of the core to the exterior of the brush layer has been recognized.[7]

Although there are a number of reports in the literature on the synthesis and self-assembly of mixed homopolymer brush-grafted (nano)particles,[11,12] none of them discussed the effect of substrate curvature on microphase separation of mixed brushes. The work presented in this Communication represents our first step toward the synthesis of mixed brushes with controlled molecular weights and narrow polydispersities on sub-100 nm silica nanoparticles and the study of the effect of substrate curvature on phase morphology of mixed brushes.

A triethoxysilane-terminated asymmetric difunctional initiator (Y-silane) was immobilized onto the surface of silica nanoparticles with an average diameter of 67 nm via an ammonia-catalyzed hydrolysis and condensation process in ethanol (Scheme 1).[11d,13] Mixed poly(*tert*-butyl acrylate) (P*t*BA)/polystyrene (PS) brushes were then grown from Y-initiator-functionalized silica nanoparticles by sequential surface-initiated atom transfer radical polymerization (ATRP) of *t*BA at 75 °C and nitroxide-mediated radical polymerization (NMRP) of styrene at 120 °C in the presence of a free initiator in each polymerization, which is an established protocol from our laboratory.[10f,11c,d] We previously confirmed that the TEMPO moiety was stable under the chosen ATRP conditions.[10c,f] By taking advantage of the "living" nature of NMRP, a series of mixed brush-grafted particle samples with the same P*t*BA M_n but different PS molecular weights were made from P*t*BA brush-grafted silica nanoparticles. The free polymers formed from the free initiators were analyzed by size exclusion chromatography (SEC), and the particles were characterized by thermogravimetric analysis (TGA) for polymer contents. We previously cleaved grafted polymers from silica particles using HF and confirmed by SEC that the molecular weights and molecular weight distributions of grafted polymers and free polymers formed from free initiators were essentially identical.[10f] By using the average size of silica nanoparticles, the molecular weights of grafted polymers[14] and the TGA data, and assuming that silica nanoparticles have the same density as bulk SiO_2, that is, 2.07 g/cm^3, the grafting densities of P*t*BA and PS were calculated. Table 1 summarizes the characterization data for three mixed P*t*BA/PS brush-grafted particle samples with P*t*BA M_n of 22.2 kDa and PS molecular weights of 18.7 kDa (MB-67-I), 23.4 kDa (MB-67-II), and 29.5 kDa (MB-67-III). The polydispersity indexes of free polymers were all <1.20. For comparison, we also include in Table 1 a mixed brush particle sample synthesized from a monochlorosilane-terminated Y-initiator-functionalized 160 nm silica particles from a prior work.[11c]

Table 1. Molecular Characteristics of Mixed P*t*BA/PS Brushes on Silica Particles and the Corresponding Free Polymers

mixed brush-grafted particle sample	PS M_n (kDa), PDI, and DP[c]	DP_{PS}/DP_{PtBA}[d]	σ_{PtBA}, σ_{PS}, and σ_{total} (chains/nm^2)[e]
MB-67-I[a]	18.7, 1.18, 180	1.04	0.54, 0.28, 0.82
MB-67-II[a]	23.4, 1.17, 225	1.30	0.54, 0.31, 0.85
MB-67-III[a]	29.5, 1.17, 284	1.64	0.54, 0.31, 0.85
MB-160[b]	18.7, 1.20, 180	0.94	0.36, 0.26, 0.62

[a]Mixed P*t*BA/PS brush-grafted silica nanoparticle samples (MB-67-I, -II, and -III) were prepared from P*t*BA brush-grafted 67 nm silica nanoparticles with P*t*BA $M_{n,SEC}$ of 22.2 kDa and PDI of 1.19 by surface-initiated NMRP of styrene at 120 °C. [b]Mixed P*t*BA/PS brush-grafted silica particle sample (MB-160) was made from P*t*BA brush-grafted 160 nm silica particles with P*t*BA M_n of 24.5 kDa and PDI of 1.11 by surface-initiated NMRP of styrene at 120 °C.[11c] [c]The values of M_n and polydispersity index (PDI) of PS were determined by SEC; the DPs of PS were calculated from M_ns. [d]The ratio of DPs of two polymers. [e]The P*t*BA and PS grafting densities (σ_{PtBA} and σ_{PS}) in each sample were calculated by using the size of silica particles, DP_{PtBA} and DP_{PS}, and TGA data corrected for the difference in the weight retentions at 100 °C between hairy particles and Y-initiator particles. The total grafting density $\sigma_{total} = \sigma_{PtBA} + \sigma_{PS}$.

For TEM study, mixed P*t*BA/PS brush-grafted silica nanoparticles were dispersed in chloroform, a nonselective good solvent for both P*t*BA and PS, and drop cast onto carbon-coated TEM grids. The TEM samples were then annealed with $CHCl_3$ vapor in a closed container for at least 3 h, followed by staining with RuO_4 at room temperature for 20 min. Note that RuO_4 selectively stains PS, making PS nanodomains appear dark and P*t*BA bright in the bright field TEM images.[11] Without staining with RuO_4, the brush layer cannot be seen,[11a] that is, only dark silica particle cores are visible under TEM. Figures 1−3 show typical top-view TEM micrographs of MB-67-I, -II, and -III, respectively. More TEM images can be found in the Supporting Information. For comparison, representative bright field TEM micrographs of mixed P*t*BA/PS brush-grafted 160 nm silica nanoparticle sample, MB-160, are included in Figure 4.

For MB-67-I, the chain lengths of P*t*BA and PS were almost the same (DP_{PS}/DP_{PtBA} = 1.04), but the grafting density of PS (0.28 chains/nm^2) was smaller than that of P*t*BA (0.54 chains/nm^2). From Figure 1A, the grafted PS chains appeared to self-assemble into isolated, truncated wedge-shaped nanodomains with a typical width at half height of ∼12 nm in the P*t*BA

dx.doi.org/10.1021/mz3003193 | *ACS Macro Lett.* 2012, 1, 1061−1065

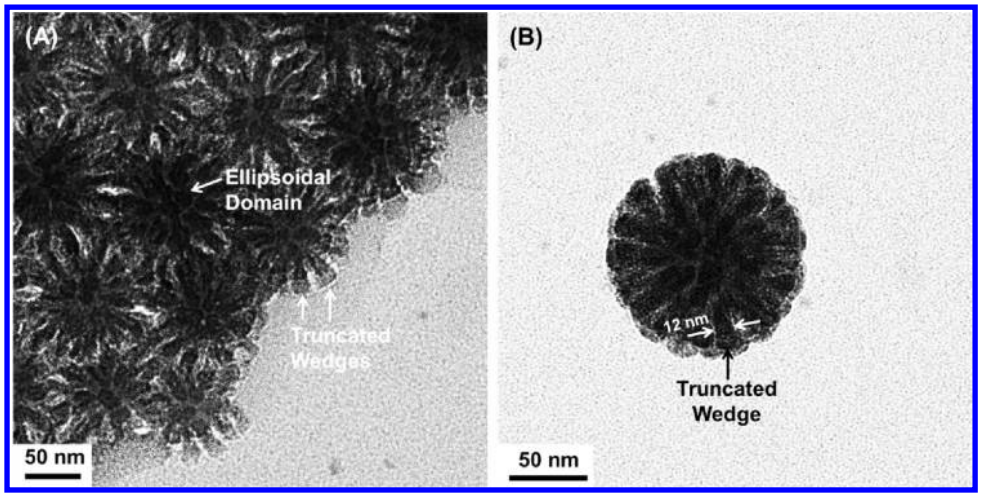

Figure 1. Top-view bright field TEM micrographs of mixed P*t*BA/PS brush-grafted 67 nm silica nanoparticles with P*t*BA M_n of 22.2 kDa and PS M_n of 18.7 kDa (MB-67-I) after being cast from $CHCl_3$ and annealed with $CHCl_3$ vapor for at least 3 h. The sample was stained at room temperature with RuO_4 vapor for 20 min.

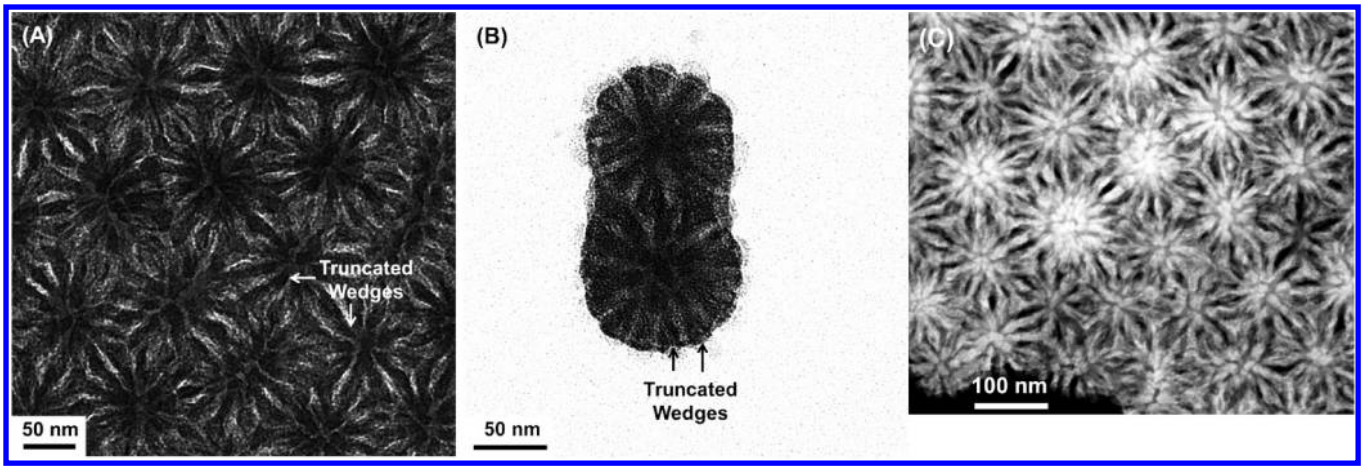

Figure 2. Top-view bright field TEM micrographs (A, B) and a top-view annular dark field scanning TEM micrograph (C) of mixed P*t*BA/PS brush-grafted 67 nm silica nanoparticles with P*t*BA M_n of 22.2 kDa and PS M_n of 23.4 kDa (MB-67-II) after being cast from $CHCl_3$ and annealed with $CHCl_3$ vapor for at least 3 h. The sample was stained at room temperature with RuO_4 vapor for 20 min.

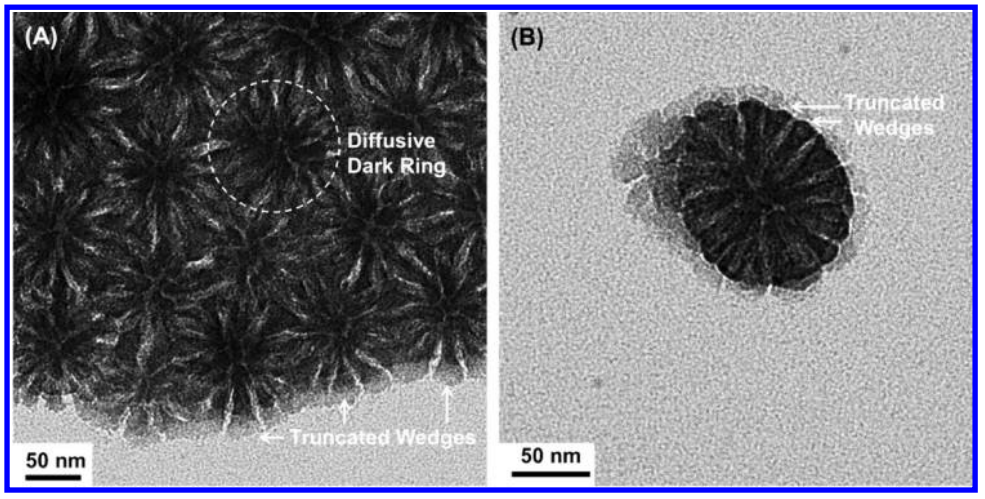

Figure 3. Top-view bright field TEM micrographs of mixed P*t*BA/PS brush-grafted 67 nm silica nanoparticles with P*t*BA M_n of 22.2 kDa and PS M_n of 29.5 kDa (MB-67-III) after being cast from $CHCl_3$ and annealed with $CHCl_3$ vapor for at least 3 h. The sample was stained at room temperature with RuO_4 vapor for 20 min.

dx.doi.org/10.1021/mz3003193 | *ACS Macro Lett.* 2012, 1, 1061−1065

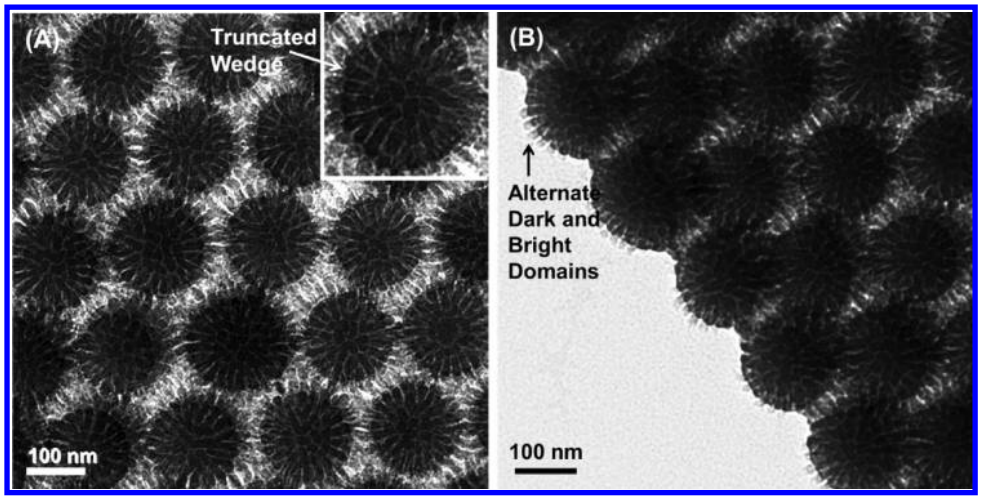

Figure 4. Top-view bright field TEM micrographs of mixed P*t*BA/PS brush-grafted 160 nm silica particles with P*t*BA M_n of 24.5 kDa and PS M_n of 18.7 kDa (MB-160) after being cast from $CHCl_3$ and annealed with $CHCl_3$ vapor for at least 3 h. The sample was stained at room temperature with RuO_4 vapor for 20 min.

matrix (see Figure 1B). These peculiar nanostructures are especially pronounced at the vacuum-brush interface (marked by arrows in Figure 1A), which were likely enhanced by the spreading of the brushes on the carbon film. Note that the TEM samples were prepared by drop casting the dispersion of hairy nanoparticles in $CHCl_3$ onto carbon-coated TEM grids. When the solvent was evaporated, the microphase separated mixed brushes collapsed, presumably vertically. Thus, the center of the particles shows the top view of PS nanodomains, which appeared to be ellipsoidal or irregular, and at or near the edge of silica nanoparticles is the side view of PS nanodomains, which are truncated wedge-shaped (Figure 1A). Because the top-view of PS nanodomains is not perfectly circular, we call them truncated wedge-shaped instead of truncated cone-shaped. Figure 1B shows the morphology of a single mixed brush-grafted silica nanoparticle; the truncated wedge-shaped nanostructures at the nanoparticle's edge can be clearly seen.

The morphology of MB-67-II was quite similar to that of MB-67-I; the truncated wedge-shaped nanostructures can be even better appreciated from the top-view bright field TEM images in Figure 2A,B than those in Figure 1. The molecular weights of two polymers in this sample were almost the same, and the grafting densities of P*t*BA and PS were 0.54 and 0.31 chains/nm^2, respectively. To some extent, the morphologies of MB-67-I and-II resemble that of MB-160 (Figure 4). Note that the molecular weights of P*t*BA and PS in MB-160 were 24.5 kDa and 18.7 kDa, respectively, and the grafting densities of P*t*BA and PS were 0.36 and 0.26 chains/nm^2, respectively. Unlike MB-67-I and -II, the nanodomains at the edge of particles in MB-160 were more uniform in the width. Although truncated wedge-shaped nanostructures can also be seen, for example, the one marked with an arrow in Figure 4A, they are much less pronounced than in Figures 1 and 2. Interestingly, alternate dark and bright nanodomains appeared at the vacuum-brush interface (marked by an arrow) in Figure 4B. These nanostructures, formed from lateral microphase separation of mixed P*t*BA/PS brushes, are nearly uniform in the width.

Figure 2C shows a top-view annular dark field scanning TEM micrograph of MB-67-II, in which the P*t*BA nanodomains appeared dark and PS was bright. Evidently, the P*t*BA nanodomains were mostly connected, forming a matrix, while bright PS nanodomains were isolated. At the edge of silica nanoparticles, the P*t*BA domains also assumed wedge shapes.

For sample MB-67-III, the PS M_n was increased to 29.5 kDa, but the grafting densities of two polymers were the same as in MB-67-II. Figure 3 shows two representative bright field TEM images. The distinct truncated wedge-shaped nanostructures remained visible, despite that the PS nanodomains became more connected and the interstitial space became darker. At the brush-vacuum interface, the truncated wedges were especially pronounced as in Figure 1. A closer examination revealed that each particle seemed to be surrounded by a diffusive dark ring as indicated by a dotted ring. The ring, though not fully closed, appeared in the center of the interstitial space. This suggests that the mixed P*t*BA/PS brushes might self-assemble into a two-layered nanostructure in which a laterally microphase separated bottom layer was covered by longer PS chains.

The observed different shapes of nanodomains formed by mixed brushes grafted on 67 and 160 nm silica particles suggest that the peculiar truncated wedge-shaped nanostructures originated from the higher curvature of 67 nm silica nanoparticles. By using the TGA data and a density of 1.05 g/cm^3 for both PS and P*t*BA and assuming that the polymer brushes formed a uniform film on the surface of silica particles, we estimated the thickness of the polymer layer in MB-67-II and MB-160 and it was 18.5 and 18.3 nm, respectively. Therefore, the periphery of a polymer-grafted silica particle is 1.6 times that of bare silica particles for MB-67-II and 1.2 times for MB-160. Due to the higher polymer content in MB-67-II (the weight retention at 800 °C was 39.8% in contrast to 63.1% for MB-160), we believe that the collapse of polymer brushes further enhanced the formation of truncated wedge-shaped nanostructures as evidenced by the pronounced features at the brush-vacuum interface in Figures 1, 3, and S2.

In summary, we synthesized mixed P*t*BA/PS brushes with controlled molecular weights and narrow polydispersities from Y-initiator-functionalized 67 nm silica nanoparticles by surface-initiated ATRP and NMRP. TEM studies showed that these mixed brushes self-assembled into distinct truncated wedge-shaped nanostructures after being cast from $CHCl_3$ and annealed with $CHCl_3$ vapor. The wedge-shaped nanostructures are particularly pronounced at the brush-vacuum interface. In contrast, under the same conditions, mixed P*t*BA/PS brushes

dx.doi.org/10.1021/mz3003193 | *ACS Macro Lett.* 2012, 1, 1061−1065

on 160 nm silica particles phase separated into nanodomains with a more uniform width. This report is the first experimental study on the effect of substrate curvature on phase morphology of mixed homopolymer brushes. We are currently synthesizing mixed brushes on various sized silica nanoparticles. A more systematic investigation on the curvature effect is underway.

■ ASSOCIATED CONTENT

Supporting Information

Experimental section; TGA analyses of bare silica nanoparticles, Y-initiator-functionalized 67 nm silica nanoparticles, and hairy nanoparticles; more top-view TEM micrographs of MB-67-I, -II, -III, and MB-160 after being cast from $CHCl_3$, annealed with $CHCl_3$ vapor, and stained with RuO_4 vapor. This material is available free of charge via the Internet at http://pubs.acs.org.

■ AUTHOR INFORMATION

Corresponding Author

*E-mail: lxz121@case.edu (L.Z.); zhao@ion.chem.utk.edu (B.Z.).

Notes

The authors declare no competing financial interest.

■ ACKNOWLEDGMENTS

This work was supported by the National Science Foundation through awards DMR-1007986 (B.Z.) and DMR-1007918 (L.Z.). The authors thank Dr. Xiaoming Jiang for the mixed brush-grafted 160 nm silica particle sample.

■ REFERENCES

(1) Marko, J. F.; Witten, T. A. *Phys. Rev. Lett.* **1991**, *66*, 1541−1544.

(2) (a) Dong, H. *J. Phys. II* **1993**, *3*, 999−1020. (b) Brown, G.; Chakrabarti, A.; Marko, J. F. *Europhys. Lett.* **1994**, *25*, 239−244.

(3) Zhao, B.; Zhu, L. *Macromolecules* **2009**, *42*, 9369−9383.

(4) Zhulina, E.; Balazs, A. C. *Macromolecules* **1996**, *29*, 2667−2673.

(5) (a) Lai, P. Y. *J. Chem. Phys.* **1994**, *100*, 3351−3357. (b) Singh, C.; Pickett, G. T.; Balazs, A. C. *Macromolecules* **1996**, *29*, 7559−7570. (c) Minko, S.; Müller, M.; Usov, D.; Scholl, A.; Froeck, C.; Stamm, M. *Phys. Rev. Lett.* **2002**, *88*, 035502. (d) Wenning, L.; Müller, M.; Binder, K. *Europhys. Lett.* **2005**, *71*, 639−645. (e) Wang, J.; Müller, M. *J. Phys. Chem. B.* **2009**, *113*, 11384−11402.

(6) Roan, J.-R. *Phys. Rev. Lett.* **2006**, *96*, 248301.

(7) Wang, Y. Q.; Yang, G. A.; Tang, P.; Qiu, F.; Yang, Y. L.; Zhu, L. *J. Chem. Phys.* **2011**, *134*, 134903.

(8) (a) Sidorenko, A.; Minko, S.; Schenk-Meuser, K.; Duschner, H.; Stamm, M. *Langmuir* **1999**, *15*, 8349−8355. (b) Minko, S.; Usov, D.; Goreshnik, E.; Stamm, M. *Macromol. Rapid Commun.* **2001**, *22*, 206−211. (c) Lemieux, M.; Usov, D.; Minko, S.; Stamm, M.; Shulha, H.; Tsukruk, V. V. *Macromolecules* **2003**, *36*, 7244−7255. (d) Santer, S.; Kopyshev, A.; Yang, H. K.; Rühe, J. *Macromolecules* **2006**, *39*, 3056−3064.

(9) (a) Minko, S.; Müller, M.; Motornov, M.; Nitschke, M.; Grundke, K.; Stamm, M. *J. Am. Chem. Soc.* **2003**, *125*, 3896−3900. (b) Ionov, L.; Minko, S.; Stamm, M.; Gohy, J. F.; Jerome, R.; Scholl, A. *J. Am. Chem. Soc.* **2003**, *125*, 8302−8306. (c) Ionov, L.; Sidorenko, A.; Stamm, M.; Minko, S.; Zdyrko, B.; Klep, V.; Luzinov, I. *Macromolecules* **2004**, *37*, 7421−7423. (d) Julthongpiput, D.; Lin, Y. H.; Teng, J.; Zubarev, E. R.; Tsukruk, V. V. *Langmuir* **2003**, *19*, 7832−7836. (e) Motornov, M.; Sheparovych, R.; Tokarev, I.; Roiter, Y.; Minko, S. *Langmuir* **2007**, *23*, 13−19. (f) Filimon, M.; Kopf, I.; Ballout, F.; Schmidt, D. A.; Bründermann, E.; Rühe, J.; Santer, S.; Havenith, M. *Soft Matter* **2010**, *6*, 3764−3768. (g) Estillore, N. C.; Advincula, R. C. *Langmuir* **2011**, *27*, 5997−6008. (h) Ochsmann, J. W.; Lenz, S.; Lellig, P.; Emmerling, S. G. J.; Golriz, A. A.; Reichert, P.; You, J.; Perlich, J.; Roth, S. V.; Beger, R.; Gutmann, J. S. *Macromolecules* **2012**, *45*, 3129−3136. (i) Price, A. D.; Hur, S.- M.; Fredrickson, G. H.; Frischknecht, A. L.; Huber, D. L. *Macromolecules* **2012**, *45*, 510−524. (j) Xiong, D. A.; Liu, G. J.; Duncan, E. J. S. *ACS Appl. Mater. Interfaces* **2012**, *4*, 2445−2454.

(10) (a) Zhao, B. *Polymer* **2003**, *44*, 4079−4083. (b) Zhao, B. *Langmuir* **2004**, *20*, 11748−11755. (c) Zhao, B.; He, T. *Macromolecules* **2003**, *36*, 8599−8602. (d) Zhao, B.; Haasch, R. T.; MacLaren, S. *J. Am. Chem. Soc.* **2004**, *126*, 6124−6134. (e) Zhao, B.; Haasch, R. T.; MacLaren, S. *Polymer* **2004**, *45*, 7979−7988. (f) Li, D. J.; Sheng, X.; Zhao, B. *J. Am. Chem. Soc.* **2005**, *127*, 6248−6256. (g) Santer, S.; Kopyshev, A.; Donges, J.; Rühe, J.; Jiang, X. G.; Zhao, B.; Müller, M. *Langmuir* **2007**, *23*, 279−285.

(11) (a) Zhao, B.; Zhu, L. *J. Am. Chem. Soc.* **2006**, *128*, 4574−4575. (b) Zhu, L; Zhao, B. *J. Phys. Chem. B* **2008**, *112*, 11529−11536. (c) Jiang, X. M.; Zhong, G. J.; Horton, J. M.; Jin, N. X.; Zhu, L.; Zhao, B. *Macromolecules* **2010**, *43*, 5387−5395. (d) Jiang, X.; Zhao, B.; Zhong, G.; Jin, N.; Horton, J. M.; Zhu, L.; Hafner, R. S.; Lodge, T. P. *Macromolecules* **2010**, *43*, 8209−8217.

(12) (a) Chiu, J. J.; Kim, B. J.; Kramer, E. J.; Pine, D. J. *J. Am. Chem. Soc.* **2005**, *127*, 5036−5037. (b) Shan, J.; Nuopponen, M.; Jiang, H.; Viitala, T.; Kauppinen, E.; Kontturi, K.; Tenhu, H. *Macromolecules* **2005**, *38*, 2918−2926. (c) Zubarev, E. R.; Xu, J.; Sayyad, A.; Gibson, J. D. *J. Am. Chem. Soc.* **2006**, *128*, 4958−4959. (d) Guo, Y.; Moffitt, M. G. *Macromolecules* **2007**, *40*, 5868−5878. (e) Cheng, J.; He, J.; Li, C.; Yang, Y. *Chem. Mater.* **2008**, *20*, 4224−4230. (f) Motornov, M.; Sheparovych, R.; Lupitskyy, R.; MacWilliams, E.; Hoy, O.; Luzinov, I.; Minko, S. *Adv. Funct. Mater.* **2007**, *17*, 2307−2314. (g) Motornov, M.; Sheparovych, R.; Lupitskyy, R.; MacWilliams, E.; Minko, S. *J. Colloid Interface Sci.* **2007**, *310*, 481−488.

(13) Ohno, K.; Morinaga, T.; Koh, K.; Tsujii, Y.; Fukuda, T. *Macromolecules* **2005**, *38*, 2137−2142.

(14) The molecular weight of P*t*BA measured by SEC relative to PS standards was used in the calculation of the P*t*BA grafting density. We previously observed that the P*t*BA molecular weights from SEC were very close to those calculated from the monomer-to-initiator ratio and monomer conversion. See refs 10f, 11c, and 11d.